GEOPHYSICS, VOL. 76, NO. 3 (MAY-JUNE 2011); P. A21–A25, 4 FIGS., 1 TABLE.
10.1190/1.3569580

Coupling ground penetrating radar and fluid flow modeling for oilfield monitoring applications

Mattia Miorali[1], Feng Zhou[2], Evert Slob[1], and Rob Arts[3]

ABSTRACT

The recent introduction of smart well technology allows for new geophysical monitoring opportunities. Smart wells, which allow zonal production control, combined with monitoring techniques capable of capturing the arrival of undesired fluids, have the potential to significantly increase the oil recovery. We consider borehole radar as a valuable technology for monitoring of the near-well region. By coupling a drainage process of a bottom water-drive reservoir with electromagnetic simulations, we find that radar sensors located in the production well can successfully map the fluid saturation evolution. In low-conductivity reservoirs ($\sigma < 0.02$ S/m), a system performance above 80 dB is necessary to record reflections in the range of 10 m. Higher conductivity values strongly reduce the radar investigation depth. Despite the technical challenges to implement a permanent down-hole radar system, the potential semi-continuous acquisition would make 4D ground-penetrating radar a promising technology in capturing the near-well fluid dynamics. Suitable environments are bottom water-drive reservoirs with thin oil layer and heavy oil reservoirs exploited by steam-assisted gravity drainage processes.

INTRODUCTION

Over the past decade, ground-penetrating radar (GPR) has become an increasingly popular tool for nondestructive characterization of the soil water content (Huisman et al., 2003; Annan, 2005). As the contrast between the dielectric constant of water and the other soil and rock components is large, the distribution of water in the subsurface strongly affects GPR wave propagation. As a result, fluid saturation changes can be monitored by time-lapse GPR measurements; successful studies for water monitoring can be found in e.g., Tsoflias et al. (2001), Talley et al. (2005), Day-Lewis et al. (2006), Deiana et al. (2008), Tsoflias and Becker (2008), and Kuroda et al. (2009) and for steam monitoring in Gregoire et al. (2006). Although the mentioned literature is mainly devoted to shallow subsurface environments, knowledge of the fluid distribution and flow is highly desired at greater depths. In the oil industry, there is a need for new monitoring techniques that could investigate the neighborhood of production wells (Bachrach et al., 2008; Davies et al., 2008). Smart well sensing technology and conventional geophysical methods such as seismics and resistivity sounding can poorly image the near-well region, whereas the increasing exploitation of unconventional and thin reservoirs requires the monitoring of this zone.

Reservoir heterogeneity and additional factors such as pressure gradients, unexpected compartmentalization and subseismic fracturing may cause an uneven fluid front and early breakthrough of undesired fluids such as water and steam in localized sections of the well. Mapping reservoir fluid saturation changes offers the possibility to detect fluid fronts in time sufficient to apply effective control strategies and, for example, to reduce production from concerned segments. Early detection and control decrease the unevenness of fluid fronts, leading to a potential increased benefit in oil production (Ebadi and Davies, 2006).

Numerical studies have already evaluated the feasibility of GPR technology for different oilfield applications (Chen and Oristaglio, 2002; Heigl and Peeters, 2005). We have proposed that an array of downhole radar sensors can satisfy the monitoring requirements in suitable oilfield environment (Miorali et al., 2011). In this paper, we carry out integrated numerical modeling where flow simulations are coupled to EM simulations. We use

Manuscript received by the Editor 5 October 2010; revised manuscript received 8 January 2011; published online 5 May 2011.
[1]Delft University of Technology-Geotechnology, Delft, Netherlands. E-mail: m.miorali@tudelft.nl; e.c.slob@tudelft.nl.
[2]China University of Geosciences-Geophysics, Wuhan, China. E-mail: zhoufeng617@gmail.com.
[3]TNO, Utrecht, Netherlands. E-mail: Rob.Arts@tno.nl.

well established mixing models to relate the evolving fluid saturation distribution and the electromagnetic (EM) properties, as proposed by Wilson et al. (2009). A numerical experiment is performed to quantify the system performance that a radar system needs to record water reflection events. We evaluate feasible investigation depths in a bottom water-drive reservoir and discuss the challenges of a potential borehole radar implementation.

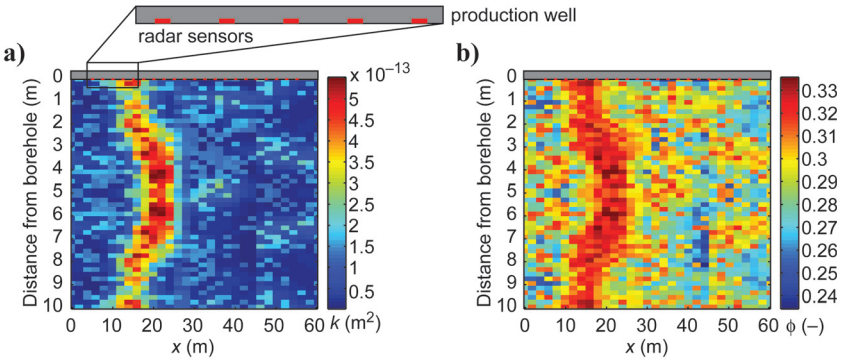

Figure 1. Spatial permeability k, expressed in m^2, (a) and porosity ϕ distribution (b). The gray box at the top of the domain represents the production well, and the radar sensors are depicted by red dots along the x direction with an interval spacing of 2.5 m.

Table 1. Reservoir and EM model properties.

Reservoir rock and fluid properties		
Properties	Value	Units
Oil compressibility	10E-9	1/Pa
Water compressibility	10E-9	1/Pa
Rock compressibility	10E-9	1/Pa
Oil density	900	kg/m^3
Water density	1000	kg/m^3
Oil viscosity	0.5E-3	Pa s
Water viscosity	1E-3	Pa s
Oil end-point relative permeability	0.9	—
Water end-point relative permeability	0.6	—
Corey exponent for oil	2	—
Corey exponent for water	2	—
Residual oil saturation	0.2	—
Connate water saturation	0.2	—
Initial reservoir pressure	40	MPa
EM rock properties		
Rock relative permittivity, ε_{rr}	7	—
Water relative permittivity, ε_{rw}	80	—
Oil relative permittivity, ε_{ro}	3	—
Water electrical conductivity, σ_w	1	S/m
Cementation exponent	2	—
Saturation exponent	2	—

Pioneering borehole radar tools fixed in the subsurface have been proposed for monitoring the movement of the water level at considerable depths (Ebihara et al., 2006; Sato and Takayama, 2007), and EM logging tools have already proved the GPR potential in imaging the neighborhood of a well (Liu et al., 2004; Mason et al., 2008). We believe our study can stimulate research in order to allow an innovative and promising application for GPR technology.

NUMERICAL EXPERIMENT

We ran a 2D numerical experiment representative of a bottom water-drive reservoir characterized by a high-permeability streak. The source of inspiration was a conceptual model analyzed by Addiego-Guevara et al. (2008): a thin sandstone reservoir containing interbedded, laterally discontinuous shale barriers that reduce the effective vertical permeability. The porosity and permeability distributions, shown in Figure 1a and b, were created using an in-house geostatistical modeling software based on principal component analysis; a large number of realizations of typical geological features were used to create the final image (Sarma et al., 2008). We considered a single horizontal production well and focused on a limited section of the reservoir close to the well; the domain was 60 m long and 10 m high.

Here we numerically solve the porous media two-phase flow equations with an implicit pressure explicit saturation (IMPES) scheme (Aziz and Settari, 1979). It is fair to note that this approach reduces the complexity of a real flow process and describes a specific production scenario. The bottom boundary is assumed to be an unlimited aquifer, whereas the top and sides as having no flow boundaries. A horizontal well is located at the top of the domain with a fixed liquid production flow rate along the entire segment. For the EM simulation, we use GprMax, a general purpose FDTD (finite difference time domain) GPR simulator (Giannopoulos, 2005). In the model, the materials are treated as lossy dielectrics, and the constitutive parameters are frequency independent. Perfectly matched layer (PML) boundary conditions have been used in order to avoid reflections from the boundaries. The source is modeled as a first derivative of a Gaussian pulse with a center frequency of 100 MHz. The radar sensors are placed in the production well and are modeled in a monostatic configuration: the EM source and receiver in the same place. In Figure 1, the gray box at the top of the domain represents the production well and the red dots the array of sensors along the well. The key parameters to run the reservoir and EM simulations are presented in Table 1. The rock and fluid properties for the flow simulations are chosen in agreement with values of similar reservoir models (Jansen et al., 2002; Addiego-Guevara et al., 2008); we refer to Miorali et al. (2011) for an analysis of the EM properties at reservoir conditions and their effect on radar wave propagation. Archie's parameters are representative of a sandstone reservoir (Archie, 1942).

The key reservoir property for determining the EM parameters is the water content θ, the product of porosity and water

saturation. To obtain the relative permittivity, for two reasons we used the complex refractive index model (CRIM) proposed by Birchak et al. (1974): It is the most widely accepted dielectric mixing model and a remarkably good agreement has been found in modeling the dielectric properties of geological materials (Knight, 2001; Seleznev et al., 2004). To obtain the effective electrical conductivity, we have used Archie's law (Archie, 1942). The CRIM model and Archie's law are the key elements in linking the reservoir and the EM simulations. As the water approaches the production well in the reservoir simulation, the distribution of the fluid saturations is extracted at predetermined times, and it is converted in EM properties distribution to allow EM simulation at those times.

RESULTS AND DISCUSSION

For every water content distribution extracted from the reservoir simulation, we ran the EM simulations. The EM response of the background medium, which is the unchanged part of the response, is subtracted from the response at each of all the subsequent stages.

Figure 2 shows a snapshot of the linking process for the 200-day reservoir simulation time. We extracted the water content distribution (Figure 2a); we converted it in EM properties, relative permittivity ε_r (Figure 2b), and electrical conductivity σ (Figure 2c); and we obtained a 2D image of the EM responses (Figure 2d). An automatic gain control was applied to enhance the reflection events at later times. As a result of the permittivity increasing between formation and the water flooded rock, the reflections present a positive main lobe, the reverse of the direct wave polarity. A qualitative comparison of Figure 2a and d reveals that the two models are effectively linked. The waterfront shape can be approximately reconstructed from the radar image.

Nevertheless, to get such an image, it would be necessary to equip the well with a dense array of radar sensors, and this may not be feasible due to the cost of the implementation. Therefore, it makes more sense to analyze the data that we can acquire from a single sensor. Figure 3 shows for few sensors, located at different x positions, the evolution of the time-lapse differences of the 1D traces. Every image represents an up-dipping event that corresponds to the advance of the waterfront. The slope of the events expresses the rate of change of the fluid distribution: a significant up-dipping slope can be interpreted as a fast water advance and a smooth slope as a slow water advance. The highest slope of the up-dipping events is observed in the image obtained from the radar sensor located in the proximity of the high permeable streak (Figure 3b).

In both Figures 2d and 3, no events are recognizable at times earlier than the waterfront reflections. This is because in the oil-saturated portion of the domain there are no changes of the water content distribution over time. Therefore, the subtraction of the electric field of the following steps with the background condition removes all the small reflections expected from the heterogeneous distribution of the EM properties.

Figure 4 shows the normalized instantaneous amplitude of the reflected events of Figure 3b in a dB scale, which represents the

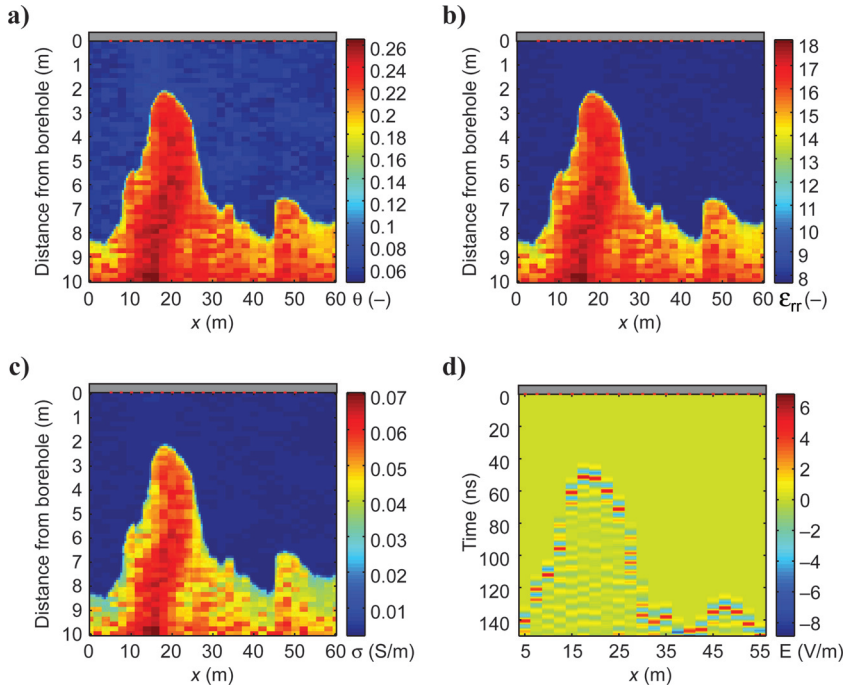

Figure 2. Snapshot of the water content θ distribution after 200 days of reservoir simulation (a) and respective relative permittivity ε_r (b) and electrical conductivity σ distribution (c). (d) The 2D radar scan; the red dots represent the radar sensors.

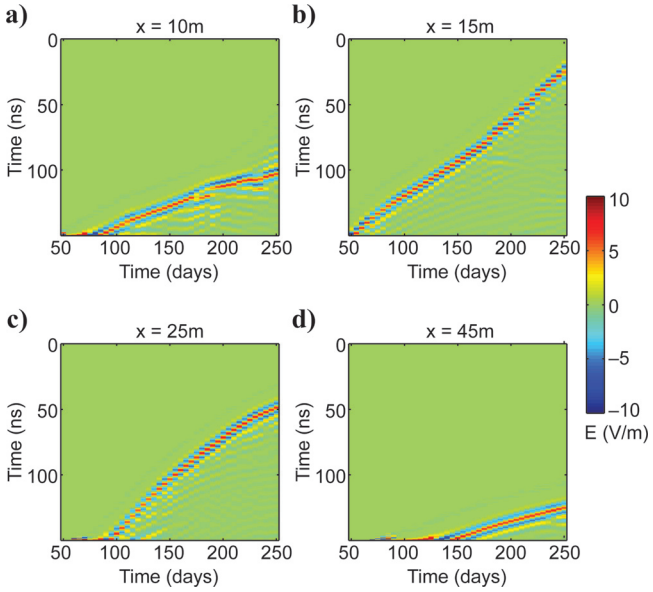

Figure 3. Evolution of the time-lapse 1D traces for different x locations of the radar sensors. For every image the y-direction represents the time in nanoseconds and in the x-direction the sequential different time steps, and the color scale represents the time-lapse amplitudes of the electric field (V/m).

system performance (SP) that a radar system would need to record the reflections. We consider the effect of different values of the formation water electrical conductivity σ_w . Figure 4a is generated with the EM parameters shown in Table 1. All the first arrivals are above −80 dB; this can be achieved with commercially available GPR technology, with system performances of about 120–160 dB (Davies and Annan, 1989). We clip all the SP values below −90 dB, which is a safe assumption for the detectability of the signal. Figure 4b-d shows SP for σ_w, respectively, equal to 2, 3, and 5 S/m. We see that the depth of investigation significantly decreases with increasing σ_w, which results in the main limitation for the implementation of down-hole radar technology.

Down-hole radar systems for oilfield applications are not currently available, but we believe the current technology has the potential to implement such systems. The main practical challenge is the metal casing interference with the EM signal. The antenna has to be in contact with the formation and separated from the metal components by a material with high dielectric constant; in this way, no metal hinders the radar wave propagation but constructively interferes with the emitted signal, as discussed by Miorali et al. (2011). This can be achieved by making suitable slots in the casing or by placing the antennas outside the casing.

Low-frequency EM noise generated by cables and radar system itself is negligible due to the high-frequency range of radar waves. Once installed, radar sensors allow semi-continuous acquisition, avoiding common 4D seismic issues such as temporal aliasing and spatial shifts. The main source of noise would be time-lapse changes of the EM properties in the background medium; this issue can be solved by increasing the data acquisition frequency relative to the rate of the local temporal changes or by enhancing the up-dipping events with an *f-k* filter.

Borehole radar measurements would extend the monitoring capability of the sensing techniques currently used in smart wells. This would result in an increase of the efficiency of the control strategies and a reduction of the uncertainties of the dynamic reservoir models (Addiego-Guevara et al., 2008; Jansen et al., 2008). The typical range of detection in the order of 10 m is particularly suitable for bottom water-drive reservoirs with thin oil layer- or steam-assisted gravity drainage processes. In this study, we consider vertical high-permeability streak as the main source of uneven fluid front; however, additional factors, such as wellbore friction or subseismic fracture may make GPR monitoring suitable in other geological scenarios.

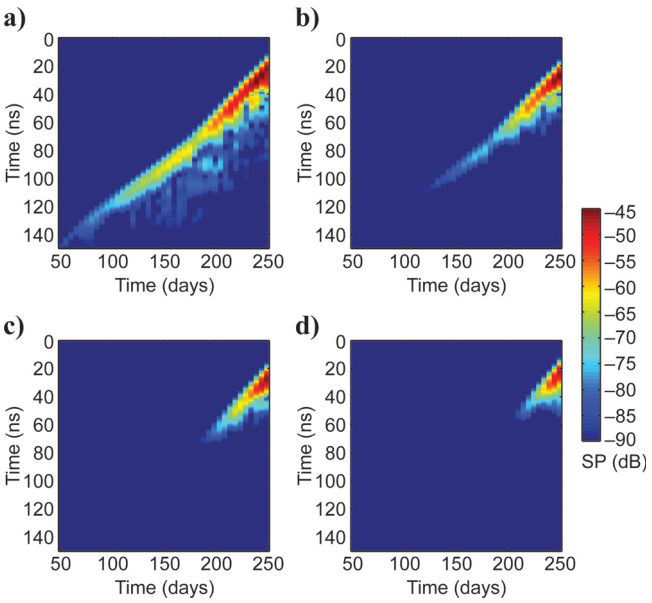

Figure 4. System performance (SP) necessary to record the reflection events at the radar sensor located at $x = 15$ m for different values of σ_w, respectively, 1 (a), 2 (b), 3 (c), and 5 S/m (d).

CONCLUSIONS

Borehole radar is a promising technique to image and monitor the near-well region of a production well. However, field trials have to be validated first by a thorough modeling study. By linking reservoir and electromagnetic simulations, it is possible to generate radar responses for realistic reservoir scenarios. The EM simulation results reveal that GPR is capable of monitoring fluid saturation changes, and a qualitative analysis is suggested to evaluate the advance of a nonuniform waterfront. Waterfront reflections in the range of 10 m are detectable in a low-conductivity reservoir environment $(\sigma < 0.02\ \mathrm{S/m})$. Formation water electrical conductivity is the main constraint to the monitoring capability of radar waves. In favorable conditions, radar measurements could be used to improve well control strategies and to constrain the reservoir models with semi-continuous monitoring data.

ACKNOWLEDGMENTS

This research was carried out within the context of the Integrated System Approach Petroleum Production (ISAPP) Knowledge Center. ISAPP is a cooperation project of Shell International Exploration and Production BV, TU Delft, and Netherlands Organization for Applied Research TNO. We thank Dr. A. Giannopoulos of the University of Edinburgh, Scotland, UK, for valuable help in the EM modeling with GprMax.

REFERENCES

Addiego-Guevara, E. A., M. D. Jackson, and M. A. Giddins, 2008, Insurance value of intelligent well technology against reservoir uncertainty: Presented at the SPE/DOE Improved Oil Symposium, SPE, 113918.

Annan, A. P., 2005, GPR methods for hydrogeological studies, *in* Y. Rubin and S. S. Hubbard, eds., Hydrogeophysics: Springer, 185–213.

Archie, G., 1942, The electrical resistivity log as an aid in determining some reservoir characteristics: Petroleum Transactions of AIME, **146**, 54–62.

Aziz, K., and A. Settari, 1979, Petroleum reservoir simulations: Applied Science Publishers.

Bachrach, R., A. Tura, and D. Wilkinson, 2008, Introduction to this special section: Permanent monitoring, smart oil fields, and reservoir surveillance: The Leading Edge, **27**, no. 12, 1614, doi:10.1190/1.3056379.

Birchak, J. R., C. G. Gardner, J. E. Hipp, and J. M. Victor, 1974, High dielectric constant microwave probes for sensing soil moisture: Proceedings of the IEEE, **62**, no. 1, 93–98, doi:10.1109/PROC.1974.9388.

Chen, Y., and M. Oristaglio, 2002, A modeling study of borehole radar for oil-field applications: Geophysics, **67**, 1486–1494, doi:10.1190/1.1512793.

Davies, D., F. Al-Khelaiwi, K. Muradov, Y. Qing, Y. Rafiei, G. Aggrey, and F. Al-Mutairi, 2008, Applications of permanent sensors for real-time well management: The Leading Edge, **27**, no. 12, 1654–1661, doi:10.1190/1.3036970.

Davies, J. L., and A. P. Annan, 1989, Ground-penetrating radar for high-resolution mapping of soil and rock stratigraphy: Geophysical Prospecting, **37**, no. 5, 531–551, doi:10.1111/j.1365-2478.1989.tb02221.x.

Day-Lewis, F., J. LaneJr., and S. Gorelick, 2006, Combined interpretation of radar, hydraulic, and tracer data from a fractured-rock aquifer near Mirror Lake, New Hampshire, USA: Hydrogeology Journal, **14**, no. 1–2, 1–14, doi:10.1007/s10040-004-0372-y.

Deiana, R., G. Cassiani, A. Villa, A. Bagliani, and V. Bruno, 2008, Calibration of a vadose zone model using water injection monitored by GPR and electrical resistance tomography: Vadose Zone Journal, **7**, no. 1, 215–226, doi:10.2136/vzj2006.0137.

Ebadi, F., and D. R. Davies, 2006, Should "proactive" or "reactive" control be chosen for intelligent well management?: Presented at the Intelligent Energy Conference and Exhibition, SPE, paper 99929, doi:10.2118/99929-MS.

Ebihara, S., K. Nagoya, N. Abe, and M. Toida, 2006, Experimental studies for monitoring water-level by dipole-antenna array radar fixed in the subsurface: Near Surface Geophysics, **4**, 89–96.

Giannopoulos, A., 2005, Modelling ground penetrating radar by GprMax: Construction & Building Materials, **19**, no. 10, 755–762, doi:10.1016/j.conbuildmat.2005.06.007.

Gregoire, C., P. K. Joesten, and J. W. LaneJr., 2006, Use of borehole radar reflection logging to monitor steam-enhanced remediation in fractured limestone — Results of numerical modelling and a field experiment: Journal of Applied Geophysics, **60**, no. 1, 41–54, doi:10.1016/j.jappgeo.2005.12.006.

Heigl, W. M., and M. Peeters, 2005, Can we obtain invasion depth with directional borehole radar?: Petrophysics, **46**, 52–66.

Huisman, J. A., S. S. Hubbard, J. D. Redman, and A. P. Annan, 2003, Measuring soil water content with ground penetrating radar: A review: Vadose Zone Journal, **2**, 476–491.

Jansen, J., A. Wagenvoort, V. Droppert, R. Daling, and C. Glandt, 2002, Smart well solutions for thin oil rims: Inflow switching and the smart stinger completion: Presented at the SPE Asia Pacific Oil and Gas Conference and Exhibition, paper 77942, doi:10.211877942-MS.

Jansen, J.-D., O. H. Bosgra, and P. M. J. Van den Hof, 2008, Model-based control of multiphase flow in subsurface oil reservoirs: Journal of Process Control, **18**, no. 9, 846–855, doi:10.1016/j.jprocont.2008.06.011.

Knight, R., 2001, Ground penetrating radar for environmental applications: Annual Review of Earth and Planetary Sciences, **29**, no. 1, 229–255, doi:10.1146/annurev.earth.29.1.229.

Kuroda, S., H. Jang, and H. J. Kim, 2009, Time-lapse borehole radar monitoring of an infiltration experiment in the vadose zone: Journal of Applied Geophysics, **67**, no. 4, 361–366, doi:10.1016/j.jappgeo.2008.07.005.

Liu, S., M. Sato, and K. Takahashi, 2004, Application of borehole radar for subsurface physical measurement: Journal of Geophysics and Engineering, **1**, no. 3, 221–227, doi:10.1088/1742-2132/1/3/007.

Mason, I. M., A. J. Bray, T. G. Sindle, C. M. Simmat, and J. H. Cloete, 2008, The effect of conduction on VHF radar images shot in water-filled boreholes: IEEE Geoscience and Remote Sensing Letters, **5**, no. 2, 304–307, doi:10.1109/LGRS.2008.915743.

Miorali, M., E. Slob, and R. Arts, 2011, A feasibility study of borehole radar as permanent downhole sensor: Geophysical Prospecting, **59**, no. 1, 120–131, doi:10.1111/j.1365-2478.2010.00904.x.

Sarma, P., L. J. Durlofsky, and K. Aziz, 2008, Kernel principal component analysis for efficient, differentiable parameterization of multipoint geostatistics: Mathematical Geosciences, **40**, no. 1, 3–32, doi:10.1007/s11004-007-9131-7.

Sato, M., and T. Takayama, 2007, A novel directional borehole radar system using optical electric field sensors: IEEE Transactions on Geoscience and Remote Sensing, **45**, no. 8, 2529–2535, doi:10.1109/TGRS.2007.898421.

Seleznev, N., A. Body, T. Habashy, and S. Luthi, 2004, Dielectric mixing laws for partially saturated carbonate rocks: SPWLA 45th Annual Logging Symposium, 1–14.

Talley, J., G. Baker, M. Becker, and N. Beyrle, 2005, Four dimensional mapping of tracer channelization in subhorizontal bedrock fractures using surface ground penetrating radar: Geophysical Research Letters, **32**, no. 4, L04401–L04405, doi:10.1029/2004GL021974.

Tsoflias, G., T. Halihan, and J. SharpJr., 2001, Monitoring pumping test response in a fractured aquifer using ground-penetrating radar: Water Resources Research, **37**, no. 5, 1221–1229, doi:10.1029/2000WR900297.

Tsoflias, G. P., and M. W. Becker, 2008, Ground-penetrating-radar response to fracture-fluid salinity: Why lower frequencies are favorable for resolving salinity changes: Geophysics, **73**, no. 5, J25–J30, doi:10.1190/1.2957893.

Wilson, V., C. Power, A. Giannopoulos, J. Gerhard, and G. Grant, 2009, DNAPL mapping by ground penetrating radar examined via numerical simulation: Journal of Applied Geophysics, **69**, no. 3–4, 140–149, doi:10.1016/j.jappgeo.2009.08.006.